

## Tuning the polarization state of light via time retardation with a microstructured surface

Shang-Chi Jiang,<sup>1</sup> Xiang Xiong,<sup>1</sup> Paulo Sarriugarte,<sup>2</sup> Sheng-Wei Jiang,<sup>1</sup> Xiao-Bo Yin,<sup>3</sup> Yuan Wang,<sup>3</sup> Ru-Wen Peng,<sup>1</sup> Di Wu,<sup>1</sup> Rainer Hillenbrand,<sup>2,4</sup> Xiang Zhang,<sup>3</sup> and Mu Wang<sup>1,\*</sup>

<sup>1</sup>National Laboratory of Solid State Microstructures and Department of Physics, Nanjing University, Nanjing 210093, China

<sup>2</sup>Nanooptics Group, CIC nanoGUNE Consolider, 20018 Donostia, San Sebastian, Spain

<sup>3</sup>NSF Nano-scale Science and Engineering Center, 3112 Etcheverry Hall, University of California, Berkeley, California 94720, USA

<sup>4</sup>IKERBASQUE, Basque Foundation for Science, 48011 Bilbao, Spain

(Received 17 February 2013; published 15 October 2013)

We report here an approach to tune efficiently the phase difference of light in two orthogonal directions,  $\Delta\varphi$ , by controlling the time retardation with a microstructured surface made of L-shaped metallic patterns. The time retardation through the judicious microstructures can be adjusted on the femtosecond level, and  $\Delta\varphi$  can be linearly tuned accurately from  $-180^\circ$  to  $180^\circ$  by changing the frequency of incident light. Particularly, the amplitudes in two orthogonal directions are identical, so that the polarization state always locates on a meridian of a Poincaré sphere. Near-field measurement confirms that there is indeed time retardation between the oscillations in the orthogonal directions of the L-shaped patterns. This approach offers an alternative way to manipulate the polarization state of light.

DOI: [10.1103/PhysRevB.88.161104](https://doi.org/10.1103/PhysRevB.88.161104)

PACS number(s): 78.67.Pt, 42.25.Ja, 42.82.-m, 78.20.Ci

The polarization state of light is determined by the amplitude and the phase relationship of two orthogonal linear vectors perpendicular to the propagation direction. Conventionally, a birefringence crystal plate along a certain crystallographic orientation and with a certain thickness, known as a wave plate, is employed to manipulate the polarization states of light.<sup>1,2</sup> The phase difference between the orthogonal components, normally termed o ray and e ray, respectively, depends on the birefringence and the thickness of the crystal plate. For natural materials, birefringence is usually small (typically, 0.1–0.2).<sup>3</sup> To achieve a certain phase shift in the orthogonal directions, the thickness of the wave plate becomes the major control parameter. For conventional optical application this can be easily accommodated. However, in integrated photonic circuits and on-chip optical devices,<sup>4,5</sup> the space is extremely restricted. Therefore, new approaches to modulate the polarization state of light are highly anticipated.

Up to now, in addition to the quasi-two-dimensional and the three-dimensional structures,<sup>6–11</sup> patterned surfaces<sup>12–15</sup> have been proposed to manipulate the polarization state. In these designs, the resonant frequencies along two orthogonal directions are different; hence the transmission light in these two directions possesses a different phase shift with respect to the incident light. However, in these studies such a function is frequency dependent,<sup>12–15</sup> which limits its applications in optical devices. Recently, a patterned interface made of an array of V-shaped antennas with different opening angles has been designed, which provides an abrupt phase shift on the cross section in the optical path and hence generates optical vortices with helicoidal wave front and orbital angular momentum.<sup>16,17</sup> To tune the polarization of light, a spatial offset is introduced to the adjacent basic subunits, which generates a phase difference between the orthogonal polarization directions. This structure changes a linearly polarized incident light to a circular polarized light corresponding to a specific offset.<sup>18</sup>

The polarization state can be graphically represented by the Poincaré sphere [Fig. 1(a)], where the equator of the

sphere represents the linear polarization states and  $P_x$  and  $P_y$  correspond to the two orthogonally linear polarization axes.<sup>1</sup> The poles of the sphere denote the right-handed and the left-handed circular polarization states, respectively. To manipulate the polarization state of light means to move the polarization state from one point to the other along a certain route on the sphere's surface. One technically beneficial approach is illustrated by two half circles marked in blue and green in Fig. 1(a), where the amplitudes in the two orthogonal directions remain identical yet the phase difference between them varies from  $0^\circ$  to  $180^\circ$  and  $0^\circ$  to  $-180^\circ$  for  $x$ - and  $y$ -polarized incidence, respectively. This scenario is illustrated in Fig. 1(b). However, currently, no structure can experimentally realize this function to the best of our knowledge.

The polarization state of electromagnetic wave depends on the phase difference between the orthogonal components  $\Delta\varphi$  as

$$\Delta\varphi = k\Delta(nd) - \omega\Delta t = k[\Delta(nd) - c\Delta t], \quad (1)$$

where  $k$  is the wave vector,  $n$  stands for the refractive index,  $d$  is the material thickness, and  $c$  and  $\omega$  denote the vacuum speed and the angular speed of light, respectively.  $\Delta(nd)$  represents the change of optical path, which is the term conventionally used for modulating the polarization state of light.<sup>1,2,6</sup>  $\Delta t$  originates from the time delay of electromagnetic radiation in the two orthogonal directions. Here we focus on the contribution of time retardation between the two arms of the L-shaped metallic pattern, which allows us to tune  $\Delta\varphi$  of the transmitted light in the range of  $-180^\circ$  to  $180^\circ$  while keeping the amplitudes of the orthogonal components identical.

An array of gold mirror-image L patterns has been designed [Fig. 2(a)]. Upon illumination of the incident light, oscillation of free electrons is excited on the perpendicularly positioned arms of the L pattern, forming two oscillating dipoles with a certain time delay. The oscillating dipoles radiate electromagnetic (EM) waves and, accordingly, change the state of the transmitted light. The transmission light is

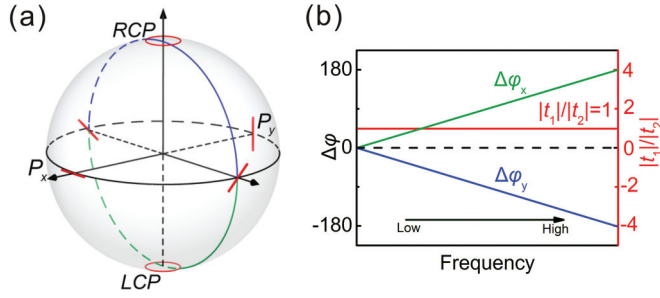


FIG. 1. (Color online) (a) The schematic micrograph of the Poincaré sphere. (b) Along the two half circles shown in (a), the amplitudes of the  $x$  and  $y$  components (represented by  $|t_1|$  and  $|t_2|$ ) are identical, yet the phase difference between them varies linearly from  $0^\circ$  to  $180^\circ$  and  $0^\circ$  to  $-180^\circ$ , respectively.

the superposition of radiation light and incident light. The optical properties of the gold structure are simulated with the software based on the finite-difference time-domain (FDTD) method before lithographic fabrication. For  $x$ -polarized normal incidence, electrons on the  $x$ -orientated arm are excited first and form an oscillating electric dipole. The oscillating  $x$  dipole then induces an oscillating dipole in the  $y$  direction with a retardation  $\Delta t$ . Therefore, the phase difference between the two components of the radiation light is generated. The polarization of the radiation can be tuned by time retardation between two dipoles, and the transmission is consequently manipulated. Due to the structural symmetry,  $y$ -polarized incident light can also induce the radiation of  $x$ -polarized light. The unique feature of this structure is that the ratio of the amplitude of electric field of  $i$ -polarized transmitted light and that of  $j$ -polarized incident light ( $i, j = x, y$ ) remains unity.

Experimentally, an array of gold L patterns is fabricated on a glass plate by electron beam lithography [EBL; Fig. 2(a)], where the thickness of the gold layer is 150 nm, the length of each arm is 900 nm, and the width is 140 nm. The size of the unit cell is 1200 nm, and the lattice constant of the array is selected to be 1350 nm. The transmittance of the sample is measured with a Fourier transform infrared spectrometer (Vertex 70v, Bruker) combined with an infrared microscope with focal plane array (FPA) spectroscopy (Hyperion 3000, Bruker), as schematically shown in Fig. 2(b). The total transmission intensity for the  $x$ - or  $y$ -polarized incidence is shown in Fig. 2(c), where  $|t_{ij}|$  stands for the amplitude of the electric field of  $i$ -polarized transmitted light induced by  $j$ -polarized incident light ( $i, j = x, y$ ). For  $x$ -polarized normal incidence, the induced  $y$ -polarized oscillation is in a broad frequency range from 87 to 130 THz [Fig. 2(d)]. Due to structural symmetry, the  $y$ -polarized incident light can also induce the radiation of the  $x$ -polarized light. Between 87 and 130 THz, the experimentally measured ratio of amplitudes of  $|t_{xx}|/|t_{yx}|$  and  $|t_{yy}|/|t_{xy}|$  are slightly higher than unity, which could be attributed to the influence of the electromagnetic loss of metal. In addition, small deviations of the  $x$  axis of the L patterns of the sample and the transmission axis of the polarizer may also lead to the asymmetry of the measured  $|t_{xx}|/|t_{yx}|$  and  $|t_{yy}|/|t_{xy}|$ .

The polarization state of light is decided by both the relative strength and the phase difference between the orthogonal

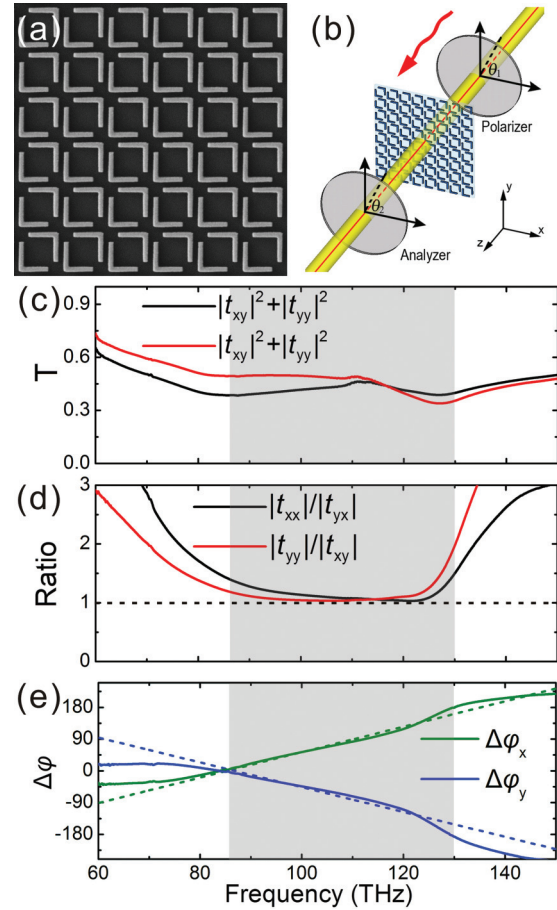


FIG. 2. (Color online) (a) SEM micrograph of the EBL-fabricated sample. The size of this micrograph is  $8.1 \mu\text{m}$ . (b) The schematics of the experimental setup for transmittance measurement. (c) The measured transmission intensity for  $x$ - and  $y$ -polarized incidence. (d) The measured amplitude ratio of the  $x$  and  $y$  components. The dashed line shows a ratio of 1. (e) The phase difference between the  $x$  and  $y$  components. The dashed lines are the linear fitting to show the linearity in the shaded region.

components. Let  $\Delta\varphi_{x(y)}$  stand for the phase of the  $y$  component of the transmission minus the phase of the  $x$  component of the transmission, where the subscript denotes the polarization of incident light. By measuring the transmission spectra with the analyzer along  $45^\circ$  and  $135^\circ$  we are able to determine  $\Delta\varphi_{x(y)}$  (see Sec. I of the Supplemental Material).<sup>19</sup> It follows that  $\Delta\varphi_x$  varies linearly from  $0^\circ$  to  $180^\circ$  and  $\Delta\varphi_y$  changes linearly from  $0^\circ$  to  $-180^\circ$  [Fig. 2(e)]. This means that with the L-patterned array shown in Fig. 2(a), the phase difference between the  $x$  and  $y$  components of the transmitted light may vary between  $-180^\circ$  and  $180^\circ$  depending on the frequency, whereas the ratio of the  $x$  and  $y$  components remains unity. Therefore, by selecting structural parameters, the microstructured surface can control the polarization state of light in a broad frequency band.

The unique properties demonstrated above can be understood from the radiation feature of the surface electric current. Upon illumination of incident light, surface electric current is excited over the metallic structure. When the lattice constant of the L-pattern array is less than the excitation wavelength, we can use the effective surface electric current density  $\vec{j}_{\text{eff}}$  to

characterize the response of the surface, which is calculated as the average of the surface electric current density in one unit cell. By solving the Maxwell equations, the radiation field corresponding to  $\vec{j}_{\text{eff}}$  is obtained as  $\vec{E}_{\text{scat}} = -\mu_0 C \vec{j}_{\text{eff}}/2$ , where  $\mu_0$  represents the permeability.<sup>20</sup>

The physical process can be understood as follows. Upon illumination of linearly polarized light, time-dependent electric charges accumulate at the ends of each arm of the L pattern, forming two perpendicularly positioned, oscillating electric dipoles. The effective inductance, resistance, and capacitance of each unit cell,  $L$ ,  $R$ , and  $C$ , characterize the dipoles in the  $x$  and  $y$  directions, respectively.<sup>21</sup> Since the dipoles in  $x$  and  $y$  directions share one corner, their coupling can be represented by a capacitance  $C'$ . It follows that

$$\begin{aligned} L \frac{d^2 Q_x}{dt^2} + R \frac{dQ_x}{dt} + \frac{Q_x}{C} &= U - \frac{Q_y}{C'}, \\ L \frac{d^2 Q_y}{dt^2} + R \frac{dQ_y}{dt} + \frac{Q_y}{C} &= -\frac{Q_x}{C'}, \end{aligned} \quad (2)$$

where  $Q_x$  and  $Q_y$  are the electric charges forming the dipoles in the  $x$  and  $y$  directions, respectively, and  $U$  represents the electric potential on the  $x$  arm generated by the electric field of  $x$ -polarized incidence. The first equation describes the resonance of the  $x$  dipole, and  $Q_y/C'$  denotes the electric potential on the  $x$  arm applied by the  $y$  dipole. The second equation describes the resonance of the  $y$  dipole, and  $Q_x/C'$  denotes the electric potential applied by the  $x$  dipole on the  $y$  arm. By solving Eqs. (2), we get

$$\begin{pmatrix} Q_x \\ Q_y \end{pmatrix} = \frac{U}{2L(\omega_0^2 - \omega^2 - \omega^2 - i\gamma\omega)} \begin{pmatrix} 1 \\ -1 \end{pmatrix} + \frac{U}{2L(\omega_0^2 + \omega^2 - \omega^2 - i\gamma\omega)} \begin{pmatrix} 1 \\ 1 \end{pmatrix}, \quad (3)$$

with  $\omega_0 = 1/\sqrt{LC}$ ,  $\omega' = 1/\sqrt{LC'}$ , and  $\gamma = R/L$ . Due to the coupling of the resonators, the resonant frequency splits to  $\sqrt{\omega_0^2 - \omega'^2}$  and  $\sqrt{\omega_0^2 + \omega'^2}$ , which correspond to the antisymmetric and symmetric modes, respectively.<sup>16,22</sup> In Eq. (3),  $Q_x$  and  $Q_y$  are not identical, which signifies the time retardation existing between the resonances of the two dipoles. The induced surface electric current on the L patterns can be obtained by making time derivative of Eqs. (3). The radiation field can be obtained by applying the energy conservation condition; that is, the sum of the transmission and reflection should equal to 1, where the transmission is the superposition of the incident light and the radiation light (see Sec. II of the Supplemental Material).<sup>19</sup> It follows that the components of the transmission matrix are expressed as

$$\begin{aligned} t_{xx} &= 1 + \frac{i\gamma\omega}{2(\omega_0^2 - \omega'^2 - \omega^2 - i\gamma\omega)} \\ &\quad + \frac{i\gamma\omega}{2(\omega_0^2 + \omega'^2 - \omega^2 - i\gamma\omega)}, \\ t_{yx} &= -\frac{i\gamma\omega}{2(\omega_0^2 - \omega'^2 - \omega^2 - i\gamma\omega)} \\ &\quad + \frac{i\gamma\omega}{2(\omega_0^2 + \omega'^2 - \omega^2 - i\gamma\omega)}. \end{aligned} \quad (4)$$

The nonzero  $t_{yx}$  indicates that the  $y$ -polarized component in the transmitted light can indeed be induced by  $x$ -polarized incidence. By fitting Eq. (4) to the experiment data, we get  $\omega' = 68.3$  THz,  $\gamma = 42.0$  THz, and  $\omega_0 = 110.6$  THz. At 87 THz ( $\sqrt{\omega_0^2 - \omega'^2}$ ), the amplitude of the antisymmetric mode reaches the maximum, the amplitude ratio  $|t_{xx}|/|t_{yx}| = 1$ , and the phase difference  $\Delta\varphi = 0^\circ$ . At the frequency of 110.6 THz ( $\omega_0$ ), the amplitude ratio is 1.004, and the phase difference is  $90^\circ$ . However, at 130 THz ( $\sqrt{\omega_0^2 + \omega'^2}$ ), the amplitude of the symmetric mode reaches the maximum. Meanwhile, the amplitudes of the two components remain identical, yet their phase difference  $\Delta\varphi = 180^\circ$ . Therefore, the amplitude ratio between the two components of the transmitted light remains unity, and the phase difference varies from  $0^\circ$  to  $180^\circ$  depending on the frequency. It should be pointed out that for  $y$ -polarized incident light, similar results can be achieved. For symmetry reasons, we have  $t_{yy} = t_{xx}$ ,  $t_{xy} = t_{yx}$ , and  $\Delta\varphi_y = -\Delta\varphi_x$ .

To show directly the time retardation between the two dipoles, transmission scattering-type scanning near-field microscopy (s-SNOM)<sup>23</sup> is applied. Due to the limitation of the available light sources, we carry out experiments on an enlarged structure (the lateral size is four times enlarged, yet the thickness remains 150 nm) at  $\lambda = 9.3$   $\mu\text{m}$  (32.3 THz). The topography of the sample is shown in Fig. 3(a). Here the phase difference between the two components of the

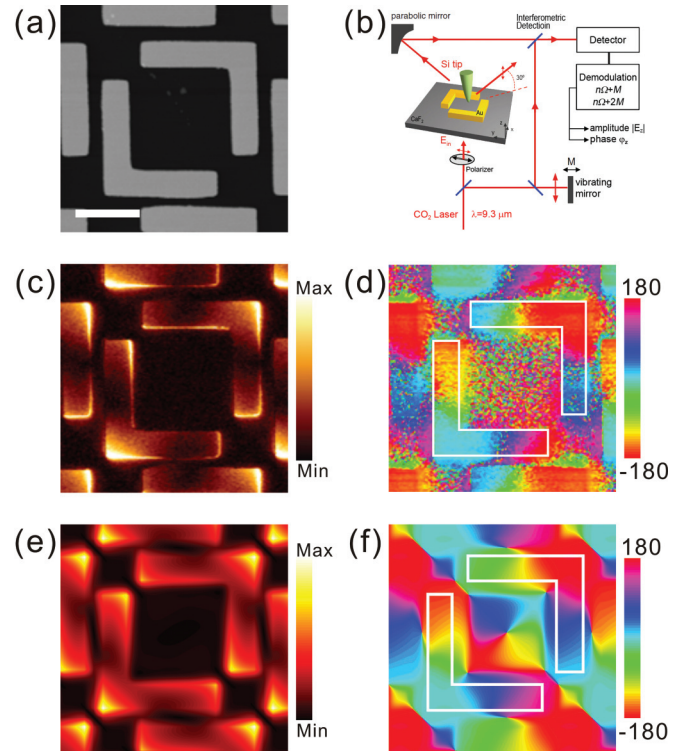


FIG. 3. (Color online) The s-SNOM investigations on the L-patterned surface. (a) The topography of the gold structures. The bar represents 2  $\mu\text{m}$ . (b) The schematics of the experimental setup of s-SNOM. (c) Amplitude  $|E_z|$  and (d) phase  $\varphi_z$  of the vertical near-field component. The incident light is  $y$  polarized ( $\lambda = 9.3$   $\mu\text{m}$ ). The simulated result of (e) the amplitude and (f) phase of  $E_z$  10 nm above the structure.

transmission light is  $-90^\circ$  for  $y$ -polarized incidence. The s-SNOM micrograph is shown in Fig. 3(b), which is obtained by illuminating the sample with a  $y$ -polarized plane wave from below under normal incidence. The near-field amplitude and phase information are obtained by mapping the light scattered from the dielectric silicon tip with a pseudoheterodyne interferometer<sup>24</sup> simultaneously with the topography imaging. Background signals are suppressed by oscillating the tip vertically at a frequency  $\Omega$  and by demodulating the detector signal at a higher harmonic  $n\Omega$  ( $n = 3$ ). The interferometric detection is realized with a vertically polarized reference field. Thus, the amplitude  $|E_z|$  [Fig. 3(c)] and phase  $\varphi_z$  [Fig. 3(d)] of the vertical near-field component are detected. For comparison, we calculate the amplitude and phase of  $E_z$  10 nm above the structure with FDTD, as illustrated in Figs. 3(e) and 3(f), respectively. The simulations are in excellent agreement with the experiments. From Figs. 3(c) and 3(d) one may find that the corners of both the  $x$  and  $y$  arms are bright, yet the phase distributions on the two arms are different. The phase of the top end of the  $y$  arm is about  $-135^\circ$  (orange in color), and the phase of the right end of the  $x$  arm is about  $135^\circ$  (pink in color), as illustrated on the bottom left L shape in Fig. 3(d). Therefore, the phase of the  $y$  dipole is about  $90^\circ$  ahead of the phase of the  $x$  dipole.

According to Eqs. (2), the oscillating  $y$  dipole can be directly excited by the  $y$ -polarized incidence. When the  $y$  dipole is pointing upwards ( $+y$  direction) and  $Q_y$  reaches the maximum value, the electric field along the  $-x$  direction is induced along the  $x$  arm, and the amplitude reaches the maximum. Consequently, the  $x$  dipole is excited, with  $Q_x$  approaching its minimum value after a certain time retardation. The induced  $x$  dipole can affect the  $y$  dipole in return, so they are strongly coupled. As indicated in Fig. 3(d), when the  $y$  dipole points upwards and the phase approaches  $0^\circ$ , the phase of the  $x$  dipole is about  $-90^\circ$ . Then after a quarter of the period time, the phase of the  $x$  dipole becomes  $-180^\circ$ , which means the  $x$  dipole points to the  $-x$  direction and the amplitude reaches the maximum. The experimental observation confirms the existence of time retardation since the oscillations of the  $x$  dipole and  $y$  dipole reach their maximum at different times.

The FPA spectroscopy is applied to measure the transmission of our structure, which confirms that the patterned surface indeed plays the role of a wave plate. Figure 4(a) shows the scanning electron microscopy (SEM) image of the sample, and the polarizer and the analyzer are arranged as shown in Fig. 2(b). The A-shaped pattern is constructed with L patterns as shown in the inset. The incident light is  $x$  polarized, and the orientation of the analyzer can be tuned. Figures 4(b) and 4(c) illustrate the images taken at a wavelength of 87 THz with  $x$ -orientated and  $y$ -orientated analyzers, respectively. In Fig. 4(b) the transmission intensity on the A pattern is lower than the surrounding glass plate since a portion of the energy of  $x$ -polarized incidence has been converted to the  $y$ -polarized radiation. In Fig. 4(c), since the glass substrate is isotropic, the substrate is dark, whereas the converted  $y$ -polarized radiation makes the A pattern brighter. Figures 4(d) and 4(e) are taken at 87 THz as well, where the phase difference between the  $x$  and  $y$  components is  $0^\circ$ . The analyzer has been set at  $\theta_2 = 45^\circ$  [Fig. 4(d)] and  $135^\circ$  [Fig. 4(e)]. In these two scenarios, the intensity passing through the substrate is the same. The zero phase difference

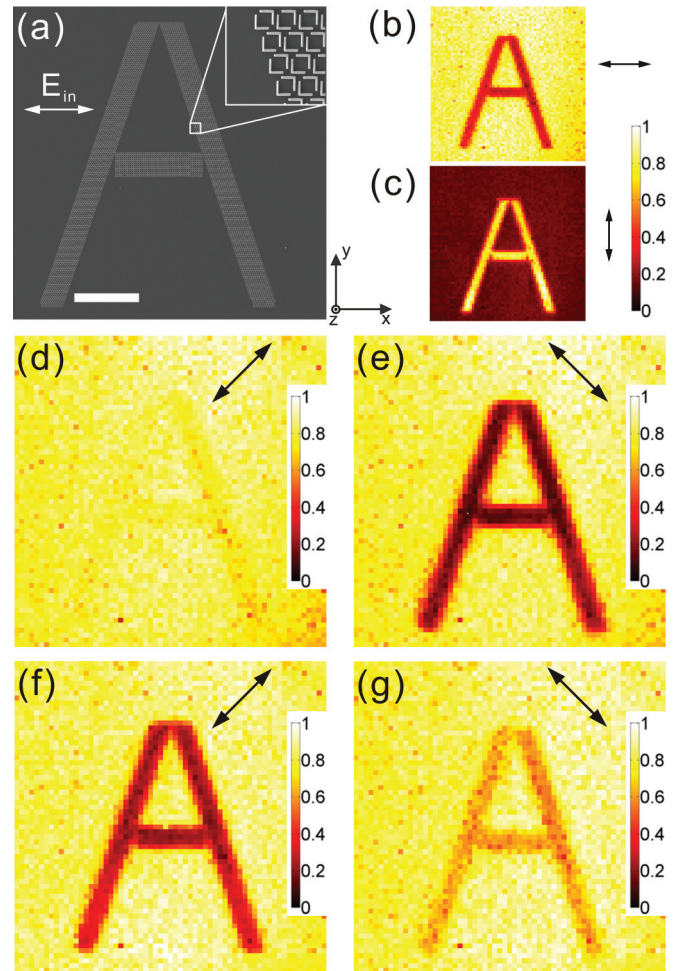


FIG. 4. (Color online) FPA measurement of the A shape made of L patterns fabricated on the glass substrate with  $x$ -polarized incidence. (a) The SEM micrograph of the sample. The bar represents  $50 \mu\text{m}$ . The arrows in (b)–(g) stand for the direction of the analyzer. (b)–(e) are the FPA images at 87 THz, where  $\Delta\varphi = 0^\circ$ , and (f) and (g) are taken at 130 THz, where  $\Delta\varphi = 180^\circ$ .

between the  $x$  and  $y$  components at 87 THz leads to the linear polarization with the polarization angle equal to  $45^\circ$ . Meanwhile, if the analyzer is arranged in the  $45^\circ$  direction, as shown in Fig. 4(d), the light intensity passing through the A pattern reaches the maximum. If, however, the analyzer is set at  $135^\circ$ , which is perpendicular to the polarization of the transmitted light [Fig. 4(e)], a dark A pattern appears. We also obtained FPA micrographs at 130 THz with the analyzer set at  $\theta_2 = 45^\circ$  [Fig. 4(f)] and  $135^\circ$  [Fig. 4(g)]. Meanwhile, the phase difference between the  $x$  and  $y$  components is  $180^\circ$  [Fig. 2(e)]. It follows that in Fig. 4(f) the A pattern becomes dark, whereas in Fig. 4(g) it turns bright, just the opposite to what is shown in Figs. 4(d) and 4(e). Figure 4 confirms that the L-patterned surface indeed converts part of the energy of  $x$ -polarized incidence to the  $y$ -polarized light and hence modulates the final polarization state.

Up to now great success has been achieved in tuning the polarization state of light with a metasurface.<sup>12–15,18,25</sup> It is essential that both the amplitude and the phase difference of the electric field in the orthogonal directions are well

under control. In our system the ratio of the amplitude in the orthogonal directions remains unity for a broad frequency band, and the phase difference between them is linearly tuned. With s-SNOM experiments, we directly verify the phase shift between the two orthogonal dipoles. This phase shift can be tuned by geometrical factors of the structure. Our study demonstrates an approach for manipulating the polarization state of light, which could be enlightening in designing integrated optical devices.

This work has been supported by the MOST of China (Grants No. 2010CB630705 and No. 2012CB921502), by the NSF of China (Grants No. 11034005, No. 61077023, and No. 11204127), by the Spanish National Project MAT2012-36580, and partly by Jiangsu Province (Grant No. BK2008012). P.S. and R.H. acknowledge financial support from the “Ikertzaileen Prestakuntza eta Hobekuntzarako Programa” promoted by the Department of Education, Universities and Research of the Basque government.

\*muwang@nju.edu.cn

<sup>1</sup>M. Born and E. Wolf, *Principles of Optics: Electromagnetic Theory of Propagation, Interference and Diffraction of Light*, 7th ed. (Cambridge University Press, Cambridge, 1999).

<sup>2</sup>E. Hecht, *Optics*, 4th ed. (Addison-Wesley, Reading, MA, 2002).

<sup>3</sup>*CRC Handbook of Chemistry and Physics*, 90th ed., edited by D. Lide (CRC Press, Boca Raton, FL, 2010).

<sup>4</sup>R. G. Hunsperger, *Integrated Optics: Theory and Technology*, 6th ed. (Springer, Berlin, 2009).

<sup>5</sup>Q. Bao, H. Zhang, B. Wang, Z. Ni, C. H. Y. X. Lim, Y. Wang, D. Y. Tang, and K. P. Loh, *Nat. Photon.* **5**, 411 (2011).

<sup>6</sup>C. Wu, H. Li, X. Yu, F. Li, H. Chen, and C. T. Chan, *Phys. Rev. Lett.* **107**, 177401 (2011).

<sup>7</sup>Z. Y. Yang, M. Zhao, P. X. Lu, and Y. F. Lu, *Opt. Lett.* **35**, 2588 (2010).

<sup>8</sup>X. Xiong, W. H. Sun, Y. J. Bao, M. Wang, R. W. Peng, C. Sun, X. Lu, J. Shao, Z. F. Li, and N. B. Ming, *Phys. Rev. B* **81**, 075119 (2010).

<sup>9</sup>N. Liu, H. Liu, S. N. Zhu, and H. Giessen, *Nat. Photon.* **3**, 157 (2009).

<sup>10</sup>X. Xiong, X. C. Chen, M. Wang, R. W. Peng, D. J. Shu, and C. Sun, *Appl. Phys. Lett.* **98**, 071901 (2011).

<sup>11</sup>X. Xiong, W. H. Sun, Y. J. Bao, R. W. Peng, M. Wang, C. Sun, X. Lu, J. Shao, Z. F. Li, and N. B. Ming, *Phys. Rev. B* **80**, 201105 (2009).

<sup>12</sup>Y. Zhao and A. Alu, *Phys. Rev. B* **84**, 205428 (2011).

<sup>13</sup>E. H. Khoo, E. P. Li, and K. B. Crozier, *Opt. Lett.* **36**, 2498 (2011).

<sup>14</sup>A. Roberts and L. Lin, *Opt. Lett.* **37**, 1820 (2012).

<sup>15</sup>J. Hao, Y. Yuan, L. Ran, T. Jiang, J. A. Kong, C. T. Chan, and L. Zhou, *Phys. Rev. Lett.* **99**, 063908 (2007).

<sup>16</sup>N. Yu, P. Genevet, M. A. Kats, F. Aieta, J.-P. Tetienne, F. Capasso, and Z. Gaburro, *Science* **334**, 333 (2011).

<sup>17</sup>X. Ni, N. K. Emani, A. V. Kildishev, A. Boltasseva, and V. M. Shalaev, *Science* **335**, 427 (2012).

<sup>18</sup>N. Yu, F. Aieta, P. Genevet, M. A. Kats, Z. Gaburro, and F. Capasso, *Nano Lett.* **12**, 6328 (2012).

<sup>19</sup>See Supplemental Material at <http://link.aps.org/supplemental/10.1103/PhysRevB.88.161104> for detailed discussions of sample fabrication, experimental measurements, and theoretical calculations.

<sup>20</sup>S. Sun, Q. He, S. Xiao, Q. Xu, X. Li, and L. Zhou, *Nat. Mater.* **11**, 426 (2012).

<sup>21</sup>J. D. Baena, J. Bonache, F. Martin, R. M. Sillero, F. Falcone, T. Lopetegui, M. A. G. Laso, J. Garcia-Garcia, I. Gil, M. F. Portillo, and M. Sorolla, *IEEE Trans. Microwave Theory Tech.* **53**, 1451 (2005).

<sup>22</sup>V. A. Fedotov, M. Rose, S. L. Prosvirmin, N. Papanimakis, and N. I. Zheludev, *Phys. Rev. Lett.* **99**, 147401 (2007).

<sup>23</sup>M. Schnell, A. Garcia-Etxarri, A. J. Huber, K. Crozier, J. Aizpurua, and R. Hillenbrand, *Nat. Photon.* **3**, 287 (2009).

<sup>24</sup>N. Ocelic, A. Huber, and R. Hillenbrand, *Appl. Phys. Lett.* **89**, 101124 (2006).

<sup>25</sup>A. Pors, M. G. Nielsen, G. D. Valle, M. Willatzen, O. Albrektsen, and S. I. Bozhevolnyi, *Opt. Lett.* **36**, 1626 (2011).